CHARACTERIZATION OF ROCK WETTABILITY THROUGH DIELECTRIC MEASUREMENTS

N. BONA, E. ROSSI and C. VENTURINI

Eni\Agip[1]

S. CAPACCIOLI, M. LUCCHESI and P. A. ROLLA

Università di Pisa[2]

CARACTÉRISATION DE LA MOUILLABILITÉ DES ROCHES AU MOYEN DE MESURES DIÉLECTRIQUES

La mouillabilité de filtres de verre et de grès de Béréa a été caractérisée par leur réponse électrique dans l'intervalle 10^2-10^8 Hz. Au moyen de traitements appropriés, la mouillabilité naturelle des matériaux a été modifiée afin d'obtenir deux séries différentes d'échantillons ayant respectivement de fortes mouillabilités à l'eau et à l'huile. Les échantillons ont été saturés à des degrés variés (pas plus de 40 %) avec de l'eau permutée ou de la saumure. Les mesures ont montré que les réponses électriques des échantillons mouillables à l'eau ou mouillables à l'huile étaient nettement différentes et plus compliquées que celles prédites par deux modèles standard. En outre, on a pu constater que la dispersivité et la tangente de pertes constituent les paramètres les plus pertinents pour caractériser la mouillabilité des échantillons.

CHARACTERIZATION OF ROCK WETTABILITY THROUGH DIELECTRIC MEASUREMENTS

The wettability of glass filters and Berea sandstone was investigated using the electric response in the interval 10^2-10^8 Hz. The natural wettability of the materials was modified to get two different sets of samples, one with strong water and the other with strong oil wettability. The samples were saturated to various degrees up to 40% with deionized water or brine. Measurements showed that the electric responses of water-wet and oil-wet samples were markedly different and more complex than those predicted by two standard models. The dispersivity and the loss tangent were found to be the most suitable parameters to check the wettability of the samples.

CARACTERIZACIÓN DE LA HUMECTABILIDAD DE LAS ROCAS POR MEDIO DE MEDICIONES DIELÉCTRICAS

La humectabilidad de filtros de vidrio y de gres de Berea se ha caracterizado por su respuesta eléctrica en el intervalo 10^2-10^8 Hz. Mediante tratamientos adecuados, la humectabilidad natural de los materiales se ha modificado con objeto de obtener dos series distintas de muestras con, respectivamente, fuertes humectabilidades al agua y al aceite. Las muestras se han saturado según diversos grados (nunca más de un 40 %) mediante agua permutada o salmuera. Las mediciones han venido a demostrar que las respuestas eléctricas de las muestras humectantes al agua o humectantes al aceite eran sumamente distintas y más complicadas que aquellas predichas por dos modelos estándar. Se ha podido así encontrar que la dispersividad y la tangente de pérdidas constituyen los parámetros más pertinentes para caracterizar la humectabilidad de las muestras.

(1) Lach Laboratories Department,
    PO Box 12069-20100 Milano - Italy

(2) Dipartimento di Fisica,
    Piazza Torricelli, 2,
    56126 Pisa - Italy

INTRODUCTION

The main reason for the interest in dielectric measurements of rocks probably lies in the possibility of investigating their physical properties in a non-destructive, rapid, accurate manner and at a relatively low cost.

Although no adequate models exist to explain experimental observations in detail, it is universally accepted that the dielectric and electrical transport properties of rocks depend on the permittivity and conductivity of fluids that saturate pores (water and oil), on their respective saturations and on how the fluids are distributed in the pore space.

One of the petrophysical properties that most affects the dielectric response of rocks is wettability. It is well known that the wetting fluid has the tendency to fill the smallest pores and to form a thin continuous film over the solid surfaces, whereas the non-wetting fluid tends to place itself mainly at the center of large pores in the form of spherical droplets. Since water and oil have very different dielectric properties, considerable differences in the dielectric spectra of rocks with different wettabilities are expected.

In order to quantify the link between dielectric properties and the wettability, a number of measurements have been performed in model porous systems: samples of sintered glass and strongly water wet and oil wet Berea sandstone. We identified the dielectric parameters that are most sensitive to wettability in the frequency range from 100 Hz to 40 MHz. It is quite surprising that the wettability is predominant over many other petrophysical properties. For example, at the frequencies investigated, the degree of water saturation and the porosity of the samples have a minor influence. This seems to indicate that in the near future it will be possible to define rock wettability through rapid and economic dielectric measurements.

1 MAIN CONCEPTS AND LITERATURE ANALYSIS

The dielectric properties of a water and oil saturated rock are expressed by the so-called "generalized complex permittivity" $\varepsilon(\omega)$:

$$\varepsilon(\omega) = \varepsilon_p(\omega) - i\frac{\sigma_{dc}}{\varepsilon_0\omega} \qquad (1)$$

where ω is the angular frequency of the electric field applied to the rock, $i = \sqrt{-1}$ is the imaginary unit, $\varepsilon_0 = 8.854 \times 10^{-12}$ farad/m is the vacuum permittivity, $\varepsilon_p(\omega)$ is the permittivity contribution of all the occurring polarization effects, σ_{dc} is the dc water conductivity. The generalized dielectric permittivity is the physical parameter which can be determined by a laboratory measurement.

Equation (1) shows that the generalized complex permittivity is the sum of two terms: the first term, $\varepsilon_p(\omega)$, consists of a real part and of an imaginary part and may be written as $\varepsilon_p(\omega) = \varepsilon_p{'}(\omega) - i\varepsilon_p{''}(\omega)$; the second term, $-i\sigma_{dc}/\omega\varepsilon_0$, is a pure imaginary quantity. Several dielectric mechanisms or polarization effects contribute to $\varepsilon_p(\omega)$: electronic, atomic, dipole and interfacial (or Maxwell-Wagner) polarization. For water and oil saturated rocks, the first three mechanisms are always activated in the frequency range we investigated (100 Hz to 40 MHz), providing a constant contribution to $\varepsilon_p(\omega)$; whereas the Maxwell-Wagner (MW) polarization, that is the dominant effect, is frequency dependent [1-5]. Therefore, in the frequency range 100 Hz-40 MHz the variation of $\varepsilon_p(\omega)$ with frequency depends essentially on the MW polarization.

The second term in Equation (1), $-i\sigma_{dc}/\omega\varepsilon_0$, is the contribution of free ions responsible for the d.c. water conductivity.

1.1 The Maxwell-Wagner Polarization

$\varepsilon_p(\omega)$ describes the interaction of matter with an external electric field. The real part of $\varepsilon_p(\omega)$ is a measure of how much energy from the electric field is stored in the matter. The imaginary part of $\varepsilon_p(\omega)$ is a measure of how dissipative or lossy the matter is in relation to the electric field.

MW polarization is activated by an electric field in heterogeneous systems, like water and oil saturated rocks. Under the effect of the electric field, the ions dissolved in the water concentrate in the regions where electrical properties undergo sudden changes. These charge concentrations produce MW polarization. MW polarization essentially occurs at the oil-water interfaces, or on pore walls. When the electric field is turned off, the ions return to their initial random distribution. The time constant that controls the process is termed relaxation time and is usually indicated by τ; the reciprocal of τ is termed the relaxation frequency. The relaxation frequency for MW polarization lies

between 10 kHz and 100 MHz, depending on the type of rock and the salinity of the water.

Figure 1 shows the trend of ε_p as a function of frequency ω of a hypothetical external electric field when MW polarization is active. At low frequencies the alternating electric field is slow enough so that the ions are able to follow the field variations. Because the polarization is able to develop fully, $\varepsilon_p{}'(\omega)$ assumes its highest value and the loss factor $\varepsilon_p{}''(\omega)$ is directly proportional to the frequency. As the frequency increases, $\varepsilon_p{}''(\omega)$ continues to increase but the storage $\varepsilon_p{}'(\omega)$ begins to decrease due to the phase lag between the fluctuations of the ions and the electric field. Above the relaxation frequency both $\varepsilon_p{}''(\omega)$ and $\varepsilon_p{}'(\omega)$ drop off as the electric field varies is too fast to influence the diffusion of the ions and the MW polarization disappears.
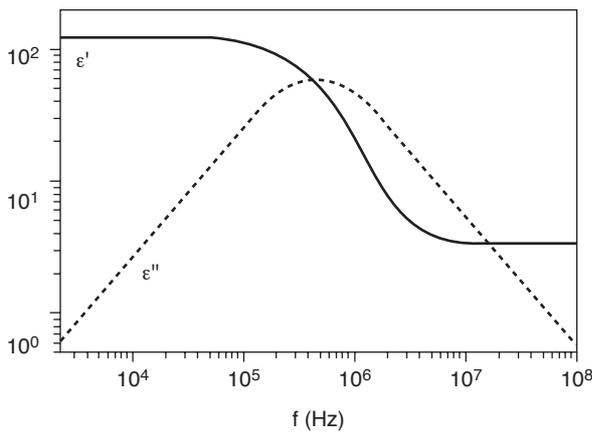

Figure 1

Frequency response of the Maxwell-Wagner polarization effect.

Rock wettability governs the dielectric response in the MW polarization frequency range. Different dielectric behaviors are therefore found, depending on the wettability of the rock, in the frequency range 10 kHz-100 MHz. These differences originate from the different distribution of water and oil in the pore space. The water is in contact with the majority of the rock surface, or is mainly confined to the center of large pores, depending on whether the rock is water wet or oil wet respectively (naturally assuming that water saturation is sufficiently low). Different relaxation times and therefore different electric responses correspond to these two different geometric configurations.

The simplest MW polarization model foresees a contribution to the rock dielectric constant in the following form:

$$\varepsilon_p(\omega) = \varepsilon_\infty + \frac{\Delta\varepsilon}{1 + i\omega\tau} \qquad (2)$$

Several characteristic relaxation parameters appear in Equation (2), such as relaxation amplitude $\Delta\varepsilon$, relaxation time τ, and the unrelaxed dielectric constant ε_∞. They depend on the electric properties and on the spatial distribution of the various constituent phases of the rock. Sillars [6] calculated these parameters for a two-phase system, consisting of an insulating phase (solid matrix and oil in the case of rocks) containing a minute amount of a disperse conducting phase (water). If the water is assumed to take the form of small, electrically non-interacting spheroidal inclusions and all the spheroids are assumed to have the same aspect ratio a/b, the Sillars' model can be applied to describe the electrical response of rocks at low water saturation. By indicating the permittivity of the insulating phase with ε_m, and the permittivity and d.c. conductivity of water with ε_ω and σ_ω, respectively, the following equations for the parameters that appear in Equation (2) are obtained by the Sillars' model:

$$\tau = \varepsilon_0 \frac{\varepsilon_m(\beta - 1) + \varepsilon_w}{\sigma_w} \qquad (3a)$$

$$\Delta\varepsilon = \frac{\varepsilon_m^2 \phi S_w g \beta^2}{\varepsilon_m(\beta - 1) + \varepsilon_w} \qquad (3b)$$

$$\varepsilon_\infty = \varepsilon_m \left[1 + \frac{(\varepsilon_w - \varepsilon_m)\phi S_w g \beta}{\varepsilon_m(\beta - 1) + \varepsilon_w} \right] \qquad (3c)$$

where ϕ is the rock porosity, S_w the water saturation, β a shape parameter of the water inclusions (for oblate spheroids $\beta = 1$, for spherical inclusions $\beta = 3$, for prolate spheroids β is very large), g is a factor that takes into account the isotropic orientation of the spheroids ($g \approx 1$ for $a/b < 10$, $g = 1/3$ for prolate spheroids).

When the rock is oil wet, the water fills the centers of the largest pores forming droplets and, therefore, $\beta = 3$. In water wet rocks, the water interfaces with the greater part of the solid surfaces and acquires the shape of very elongated spheroids, therefore $\beta \gg 3$. By introducing these values in Equation (3b) it is found that, for an equal water saturation, the relaxation amplitude $\Delta\varepsilon$ is

much greater in a water wet rock than in an oil wet rock. By introducing these values in Equation (3a) it is found that water wet rocks have much longer relaxation times t than oil wet rocks for an equal σ_w.

1.2 Lysne's Model and Other Effects

A more complicated response than that in Equation (2) is frequently found in experimental data [7]. For this reason Lysne [8] extended Sillars' model to porous systems in which the aqueous inclusions have a given distribution of the shape factor β. The result is expressed by the following dielectric constant:

$$\varepsilon_p(\omega) = \varepsilon_\infty + \int_0^\infty \frac{\Delta\varepsilon(\tau)d\tau}{1 + i\omega\tau} \qquad (4)$$

where $\Delta\varepsilon(\tau)$ is the same quantity as in Equation (2), but β, g and S_w now refer to the contribution of the inclusions with characteristic time τ. The Lysne model does not overcome any of the limits of Sillars' model, but has a greater versatility. For example, if conducting phases of different conductivity si are present, their contribution is added in Equation (4) and $\Delta\varepsilon(\tau)$ represents the general distribution of relaxation times. Any dielectric function can be described by Equation (4) using a suitable distribution of the relaxation times. Unfortunately, it is very difficult to trace the microscopic properties of the rock starting from $\Delta\varepsilon(\tau)$, since a bi-univocal relationship no longer exists.

Several measurements on sandstones [3] and [9-12] have indicated behaviors that cannot be described by Equation (1). They involve the so-called Power Law effects (PL). It is necessary to add further terms to the generalized dielectric permittivity in these cases, to obtain an adequate simulation of the electric response of the rock, expressed as:

$$\varepsilon_{PL}(\omega) = A \frac{(i\omega)^{N-1}}{\varepsilon_0} \qquad (5)$$

with A = constant and $0 \leq N \leq 1$. Response (5) is typical of a large number of disordered solids, where the charge carriers are weakly bound or confined in regions of low mobility [13-15]. Electrical transport is a discontinuous process in these systems, due to charge hopping from one site to another. PL mechanisms indicate a progressively increasing conductivity $\sigma'(\omega) = \omega \cdot \varepsilon_0 \cdot \varepsilon_{PL}''(\omega)$ with frequency, whereas storage $\varepsilon_{PL}'(\omega)$ decreases constantly with frequency. A peculiar

characteristic of Equation (5) is that the phase is independent of frequency. Normally, two different regimes are present in systems that manifest PL behavior: a low frequency regime $(0 < N < 0.5)$ associated with long range charge diffusion processes [9, 10, 11], and a high frequency regime $(0.5 < N < 1)$ associated with short range conduction mechanisms [3, 12, 16, 17].

2 EXPERIMENTAL

2.1 Materials

The aim of this study was to investigate the effects of wettability on the dielectric response of rocks. Measurements were taken on 8 samples of Berea sandstone and on 16 sintered glass filters, with two different mesh sizes. Figure 2 shows the volumetric distribution of the pore radii measured for one of the Berea samples, and for two glass filters of different mesh size.

Our experiment consisted of modifying the original strong water wettability of half of the samples, making them oil wet. The electric impedance and dielectric constant of all the samples were then measured. The aim of the study was to verify the presence of systematic differences in the dielectric response of the rock, as a function of wettability.
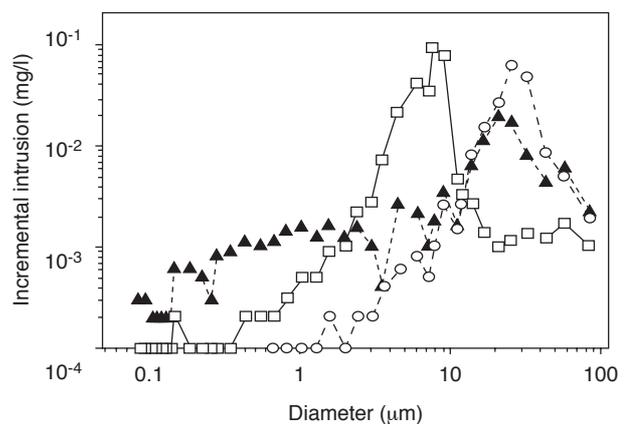

Figure 2

Volumetric distribution of pore radii of three samples that were analyzed. Dashed line and open circles: sintered glass filter (mesh 3). Solid line and open squares: sintered glass filter (mesh 4). Dotted line and solid triangles: Berea sandstone sample.

The samples to be made oil wet were silanized using a method published by N. E. Takach *et al*. [18]. The method involves incorporating the vapor of bis(dimethylamino)dimethylsilane onto the solid surfaces of the samples at a temperature of 290°C in a vacuum oven. It proved to be the only efficient way to produce a strong oil wet condition among the many tested. These included aging the samples in crude oil, fluxing with asphaltenes and other silanization processes.

TABLE 1

Characteristics of the analyzed samples.
The following conventions were adopted: O = oil wet;
W = water wet; D = deionized water; B = brine

	Wettability	Water type	Porosity (%)	S_w (%)	Amott index Water	Oil
Sample: glass - mesh size = 3 (g3)						
g3A	O	D	36.2	5.9		
g3B	O	D	38.8	7.7		
g3C	O	B	37.9	2.6	0.00	0.85
g3D	O	B	36.5	3.0		
g3E	W	D	34.9	4.2		
g3F	W	D	35.7	3.9		
g3G	W	B	31.0	6.4	0.88	0.00
g3H	W	B	32.6	8.3		
Sample: glass - mesh size = 4 (g4)						
g4A	O	D	37.6	9.6		
g4B	O	D	38.3	9.4		
g4C	O	B	30.3	7.5		
g4D	O	B	29.6	7.8	0.00	0.48
g4E	W	D	41.6	5.0		
g4F	W	D	38.0	8.5		
g4G	W	B	44.2	8.6		
g4H	W	B	40.1	6.0	0.91	0.00
Sample: Berea (be)						
beA	O	D	19.8	34.2		
beB	O	D	20.0	36.0		
beC	O	B	19.1	44.6	0.00	0.39
beD	O	B	19.4	36.1		
beE	W	D	21.8	22.3		
beF	W	D	21.7	20.1		
beG	W	B	21.7	18.4		
beH	W	B	21.4	21.9	0.39	0.00

All the samples were water saturated; a part of the water was then displaced by oil, until relatively low water saturations were obtained. Deionized water was used for 50% of the samples, brine with 75.8 g/l NaCl salinity was used for the remaining 50%. The oil that was used was soltrol, an iso-paraffinic oil produced by Phillips. Soltrol has an ideal dielectric behavior, maintaining a static dielectric constant throughout the frequency range investigated and with negligible losses.

Table 1 shows the petrophysical characteristics of the samples that were analyzed (the Amott wettability index is available for 6 samples). Table 2 shows the electrical properties of the fluids that were used.

TABLE 2

Electrical properties of the materials (25°C)

	Static dielectric const. (adimens.)	100 Hz conductivity (S/m)
Dry matrix	3-7	$< 5 \times 10^{-9}$
Deionized water	78.8	1.57×10^{-3}
Brine	67.0	9.5
Soltrol	2.015	-

2.2 Measurement Set-Up and Experimental Procedure

The complex impedance of the 24 samples listed in Table 1 was measured in the frequency range 100 Hz-40 MHz, using a HP 4194A Impedance Analyzer. The temperature was kept constant at 25.0 °C and controlled to within 0.1 °C during the measurements. A voltage of 0.1 V was applied. All the analyzed samples were disk shaped: some had a diameter of 2.5 cm, others of 5 cm; their thickness varied between 0.5 cm and 0.9 cm. To measure the impedance, the samples were put into a parallel golden plate capacitor specifically designed for the experiment. A two-contact standard method was used. Figure 3 shows the experimental apparatus and the associated electrical circuit.

The Impedance Analyzer measures the total impedance Z_T of the equivalent circuit illustrated in Figure 3. Z_T is the sum of two contributions in series: the impedance Z_C, which accounts for the capacitance of the cell and of the interconnecting wires, and the series impedance Z_L of the inter-connecting system. Z_L may be measured directly by short-circuiting the cell. Z_C is then calculated by the difference (Z_T-Z_L).
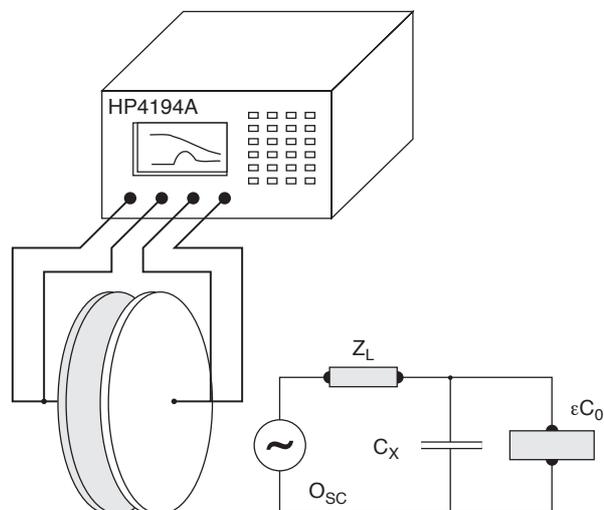
Figure 3

Experimental apparatus. The sample to be analyzed is placed between the plates of a flat capacitor and connected to the Impedance Analyzer. The equivalent circuit is also shown.

By introducing standard samples of known dielectric permittivity into the cell, we found that the complex admittance $Y_C = (Z_C)^{-1}$ can be expressed as:

$$Y_c(\omega) = i\omega C_0 \varepsilon(\omega) + i\omega C_x \qquad (6)$$

where C_0 is the capacitance of the empty cell, $\varepsilon(\omega)$ is the generalized dielectric permittivity of the sample, and C_x is the total spurious capacitance due to fringing effects, to possible stray capacitance and to the capacitance in the wiring. When a sample of unknown permittivity is put in the capacitor we can calculate its permittivity by taking two admittance measurements. First, we measure the admittance of the empty capacitor $Y_0(\omega)$, and then the admittance $Y_C(\omega)$ of the capacitor with the sample inside. The dielectric permittivity $\varepsilon(\omega)$ of the sample is obtained using Equation (6):

$$\varepsilon(\omega) = 1 + \frac{Y_c(\omega) - Y_0(\omega)}{i\omega C_0} \qquad (7)$$

Figure 4 shows that the impedance $Z_r = (i\,\omega\,\varepsilon\,C_0)^{-1}$ is, in turn, the sum of two contributions in series: the impedance Z_S of the sample introduced in the capacitor and the impedance Z_I associated with the electrode-sample interface. This effect is due to electrode polarization. Z_I can greatly affect the permittivity values measured using a two-electrode method [19].

Our results show that the impedance Z_I at the interface only makes a significant contribution in the brine saturated water wet samples.

In these cases we found a Power Law frequency behavior for Z_I of the type: $Z_I = K/(i\omega)^M$ with $M \in [0.5, 0.7]$. Such behavior for Z_I is commonly found in many studies on ionic conductors using blocking electrodes and on rock samples saturated with brine [3]. On the other hand, we found negligible Z_I values for the oil wet and the water wet samples saturated with deionized water.
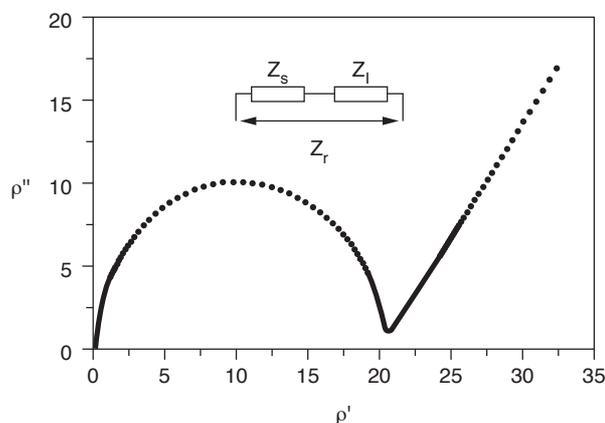

Figure 4

Electrode polarization. An impedance Z_I due to electrode polarization sums to the sample impedance Z_S; the corresponding Argand plot and equivalent circuit are displayed.

Figure 5 shows the Argand plots for four of the samples that were analyzed. The plots graphically display the imaginary part of the complex resistivity $-\rho_a''(\omega)$ versus the real part $\rho_a'(\omega)$. The complex resistivity was calculated from the impedance Z_r, as $\rho_a = Z_r \cdot A/l$, where A and l are the cross-section and thickness of the analyzed sample, respectively.

Plots with a single circle arc, such as those produced by the oil wet samples (Fig. 5 (a) and (b)), indicate the absence of interface effects. In these cases the impedance Z_I is negligible, whereas electrode polarization was found in the water wet brine saturated samples with a greater conductivity (Fig. 5 (c) and (d)). At low frequencies, the circle arc degenerates to a
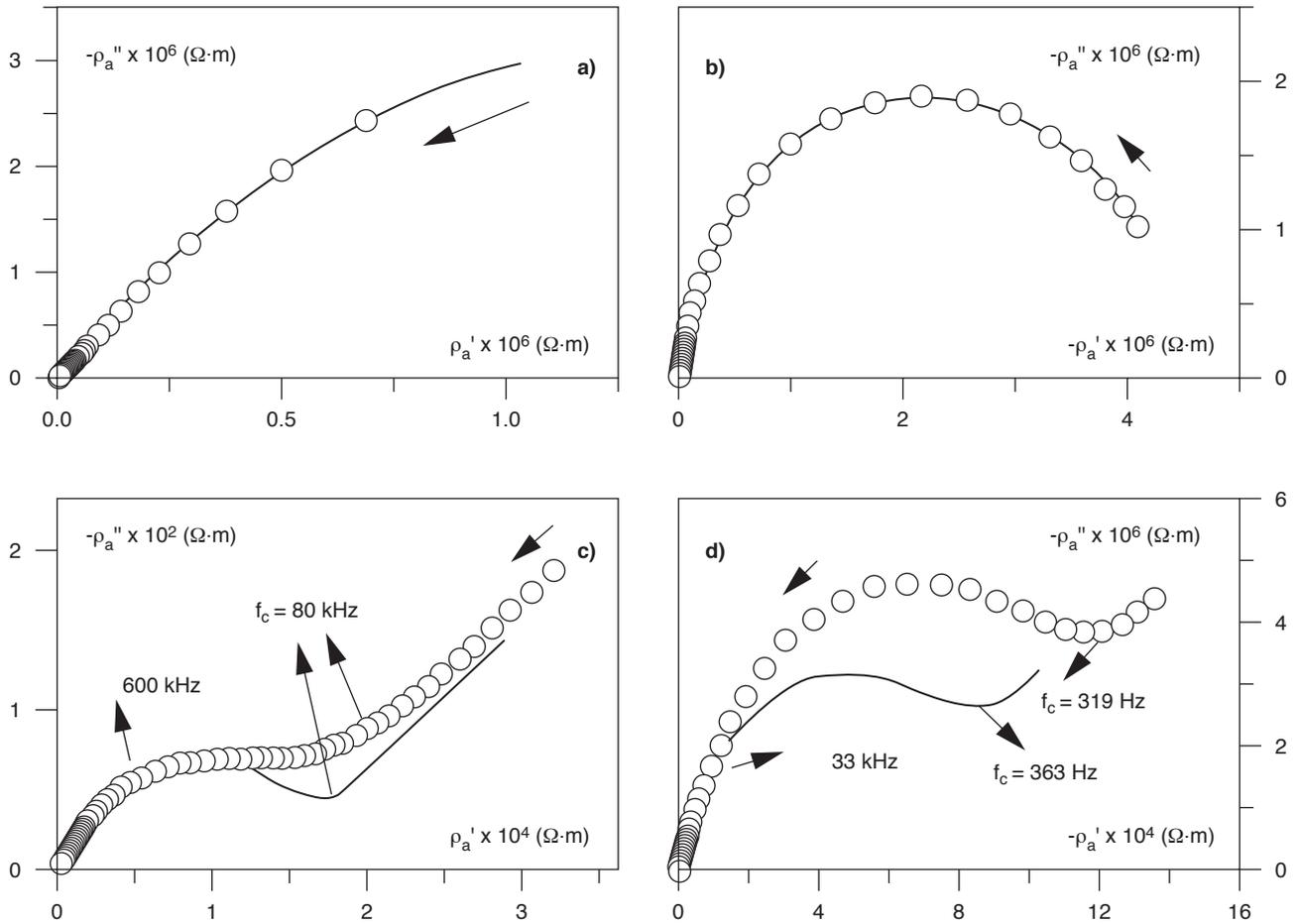
Figure 5

Argand plots: imaginary part $-\rho_a''$ of the resistivity as a function of the real part $\rho_a'(\omega)$. a) Oil wet Berea (beD) saturated with brine; b) oil wet glass (g3D) saturated with brine; c) water wet Berea (beH) saturated with brine; d) water wet glass (g3G) saturated with brine. Continuous line: measurements made with applied voltage of 1 V (r.m.s.); open dot: measurements made with applied voltage of 0.1 V (r.m.s.).

straight line due to the Power Law response of Z_I. As can be seen, a critical frequency exists, f_c, for which $-\rho_a''(\omega)$ has a minimum value; f_c is approximately inversely proportional to the sample resistivity.

3 RESULTS AND DISCUSSION

Figure 6 shows the behaviors, as a function of frequency, of the real part ε' and the imaginary part ε'' of the generalized dielectric permittivity.

The plots refer to four glass samples (mesh size 4). Two of these are water wet and two are oil wet. The samples were saturated with deionized water and brine, in order to obtain all the four possible combinations of wettability and water type:
– oil wet sample saturated with deionized water;
– oil wet sample saturated with brine;
– water wet sample saturated with deionized water;
– water wet sample saturated with brine.

Analogous quantities relating to four Berea samples are detailed in Figure 7. All the Berea samples, the glass samples of mesh size 4 and the glass samples of mesh size 3, whose response is not shown, gave the same results. The measured spectra and the spectra corrected for the electrode polarization contribution (solid line), where present, are shown in the figures.

3.1 The effect of wettability

From a study of the plots, it can be noted how wettability clearly affects the dielectric properties of the samples that were analyzed. The water wet samples show significantly higher values of ε' and ε'' than the corresponding oil wet samples. At low frequency all the

samples show the value of ε'' decreasing with increasing frequency; this effect is due to dc conductivity. At higher frequencies the behavior of ε'' differs depending on sample wettability. In oil wet samples a maximum value is clearly visible in the region of frequencies where Maxwell-Wagner relaxation would be expected; in water wet samples the loss peak associated with MW relaxation is never clearly visible and ε'' has a constantly decreasing trend. Although masked by other effects, the MW peak manifests itself by weak changes in the slope of ε''.

3.2 The effect of water conductivity

As for the effect of the water type, it must be noted that each of the brine saturated samples shows a value of the MW relaxation frequency that is higher than that found for the samples saturated with deionized water. From a qualitative point of view, this is consistent with Equation (3a), which suggests that the greater the relaxation time, the lower the water conductivity. There is not, however, good consistency from a quantitative point of view. When calculating the ratio of the MW
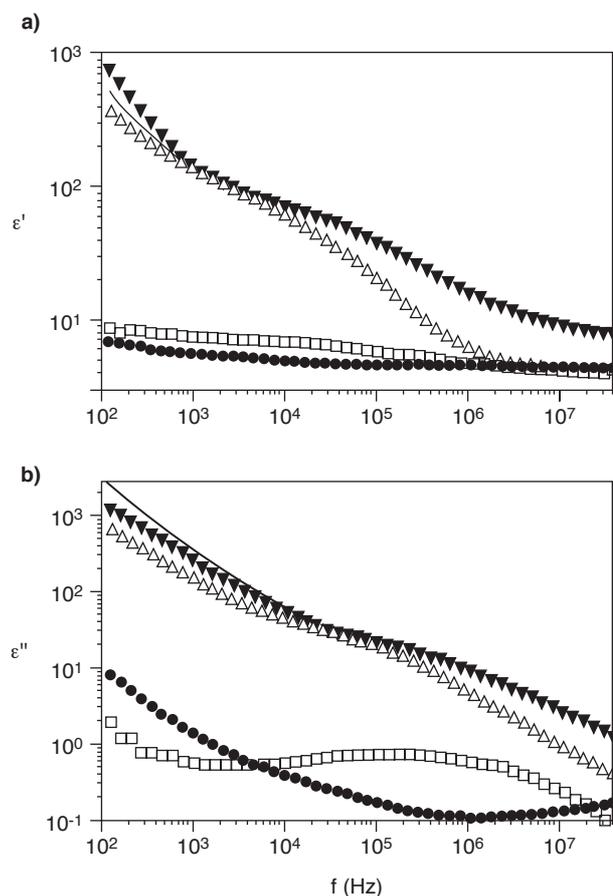

Figure 6

a) Log-log plot of the real part ε' of the permittivity as a function of frequency for glass (mesh 4).

b) Log-log plot of the imaginary part ε'' of the permittivity as a function of frequency for glass (mesh 4). Open square: oil wet sample saturated with deionized water (g4A). Solid dot: oil wet sample saturated with brine (g4D). Open up triangle: water wet sample saturated with deionized water (g4F). Solid down triangle: water wet sample saturated with brine (g4G). Solid line: data corrected for electrode polarization.
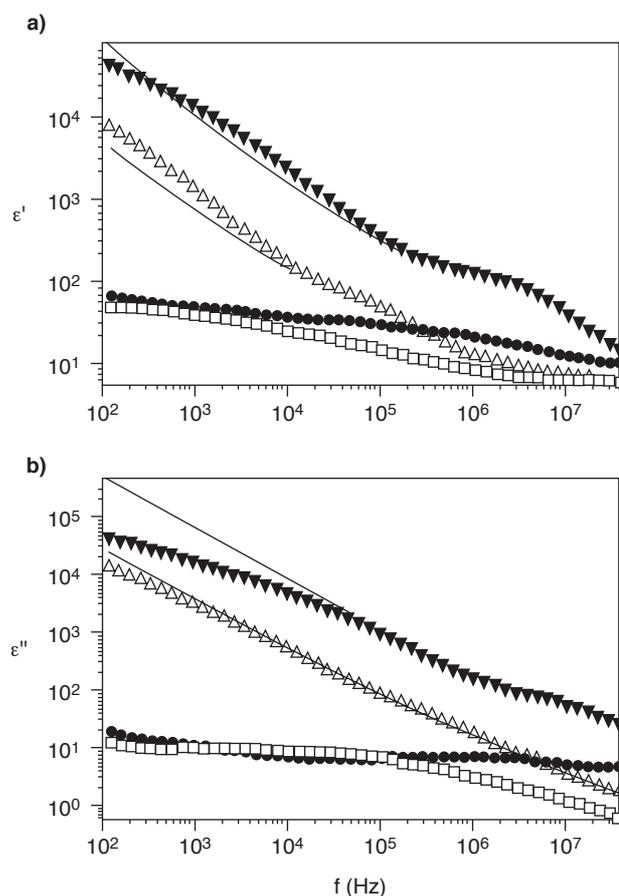
Figure 7

a) Log-log plot of the real part ε' of the permittivity as a function of frequency for Berea.

b) Log-log plot of the imaginary part ε'' of the permittivity as a function of frequency for Berea. Open square: oil wet sample saturated with deionized water (beB). Solid dot: oil wet sample saturated with brine (beC). Open up triangle: water wet sample saturated with deionized water (beF). Solid down triangle: water wet sample saturated with brine (beH). Solid line: data corrected for electrode polarization.

peak frequencies for samples having the same type of wettability and water saturation, we find a value that is not inversely proportional to the ratio of the water conductivities, as Equation (3a) would predict. In short, the models we have referred to can provide a qualitative picture of the phenomena, but they are not able to give a satisfactory quantitative description. Accordingly, a more complex model should be tested [20].

3.3 Analysis of the Dispersivity

Water wet samples show more markedly dispersive spectra than do oil wet samples. In other words, the variation of permittivity with frequency is much higher. Dielectric permittivity logarithmic derivatives, D_1 and D_2, have been used for a more detailed analysis of this aspect:

$$D_1 = \frac{\partial\left\{Log_{10}\left[\varepsilon'(\omega) - \varepsilon_\infty\right]\right\}}{\partial\left\{Log_{10}[\omega]\right\}} \qquad (8a)$$

$$D_2 = \frac{\partial\left\{Log_{10}\left[\varepsilon''(\omega)\right]\right\}}{\partial\left\{Log_{10}[\omega]\right\}} \qquad (8b)$$

The quantities D_1 and D_2 represent the slopes of curves ε' and ε'', when plotted in a bilogarithmic plot versus frequency. The greater the permittivity variation with frequency, the greater the absolute values of D_1 and D_2. Equivalent parameters to D_1 and D_2 have already been used by other authors [10 and 21]. The behaviors of D_1 and D_2 as a function of frequency are shown in Figures 8 and 9 for the four sample classes (oil wet glass, water wet glass, oil wet Berea, and water wet Berea).

The behavior of the oil wet samples is clearly distinguishable from that of the water wet samples. The average absolute value of D_1 and D_2 for the oil wet samples is significantly lower than the value found for the water wet samples. The petrophysical characteristics of the samples (porosity and water saturation level) and the electrical characteristics of the saturating water (conductivity) shift the curve peaks and modify the shape, but leave the overall behavior of electrical response unchanged.

Considering the curves in Figures 8 and 9, it appears that Equation (1) does not permit an accurate description of the observed responses. This is particularly evident for the water wet samples.

According to Equation (1), the imaginary part of the generalized permittivity $\varepsilon''(\omega)$ is equal to $\varepsilon''_p(\omega) + \sigma_{dc}/(\varepsilon_0\,\omega)$.

This relationship reduces to $\varepsilon''(\omega) \cong \sigma_{dc}/(\varepsilon_0\,\omega)$ at low frequencies (assuming that σ_{dc} is high enough), which results in a dispersivity $D_2 = d(Log\,\varepsilon'')/d(Log\,\omega)$ approximately equal to -1, provided the d.c. conductivity is frequency independent.

Our experiments, however, show that the dispersivity D_2 of both Berea samples and glass filters is greater than -1. If we look at the brine saturated samples, for instance, we observe a low frequency plateau where:
- $D_2 \cong -0.8$ in the frequency range 100 Hz-1 kHz for the water wet glass filter (Fig. 8).
- $D_2 \cong -0.9$ in the frequency range 100 Hz-300 kHz for the water wet Berea sample (Fig. 9).

Analogous results were found for each of the water wet samples analyzed (whose behavior is not shown here). This response is clearly not consistent with Equation (1). To model the observed behavior, an additional term of the form:

$$\varepsilon_{PL}(\omega) = A(i\omega)^{N-1}/\varepsilon_0\,(0 < N < 1)$$

must be added to the generalized permittivity $\varepsilon(\omega)$.

Thus:

$$\varepsilon(\omega) = \varepsilon_p(\omega) - i\sigma_{dc}/\left(\varepsilon_0\,\omega\right) + A(i\omega)^{N-1}/\varepsilon_0 \qquad (9)$$

In so doing, the imaginary part of $\varepsilon(\omega)$ becomes:

$$\varepsilon''(\omega) = \varepsilon''_p(\omega) + \sigma_{dc}/\left(\varepsilon_0\,\omega\right)$$
$$+ A\sin\left[(1-N)\pi/2\right]\omega^{N-1}/\varepsilon_0$$

which reduces to:

$$\varepsilon''(\omega) = \sigma_{dc}/\left(\varepsilon_0\,\omega\right)$$
$$+ A\sin\left[(1-N)\pi/2\right]\omega^{N-1}/\varepsilon_0$$

at low frequencies. As mentioned in Section 1.2, this relationship accounts for a Power Law effect. Such an effect is typical of clay rich systems, although it has also been observed on clay free samples, and is consistent with other published data (see, for instance, reference [10] which presents values of D_2 ranging between -0.99 and -0.95).

It is interesting to note that at low frequencies the Power Law effect can dominate the dielectric response of the sample. Equation (9) suggests that in this case the generalized permittivity reduces to:

$$\varepsilon(\omega) \cong A(i\omega)^{N-1} / \varepsilon_0 \qquad (9d)$$

According to this approximation, the dispersivity parameters are expected to be $D_2 \cong D_1 \cong N\text{-}1$ when $\omega \rightarrow 100$ Hz. This prediction agrees with our results; both water wet Berea and glass samples show, in fact, values of D_1 very close to those of D_2 at low frequencies. This effect does not occur in oil wet samples, whose D_1 always falls in the range [–0.3, 0] (low dispersivity) while D_2 tends to lower values. The stronger contribution of the Power Law effect in the water wet samples is responsible for the observed higher dispersivity. Considering the curves in Figures 8 and 9, it appears that the PL effect is still active at higher frequencies, although it is no longer dominant. As can be seen, the maximum of D_2, associated with the occurring MW relaxation, is positive for the oil wet samples (as for an ideal MW peak), whereas it is well below zero for the water wet samples.
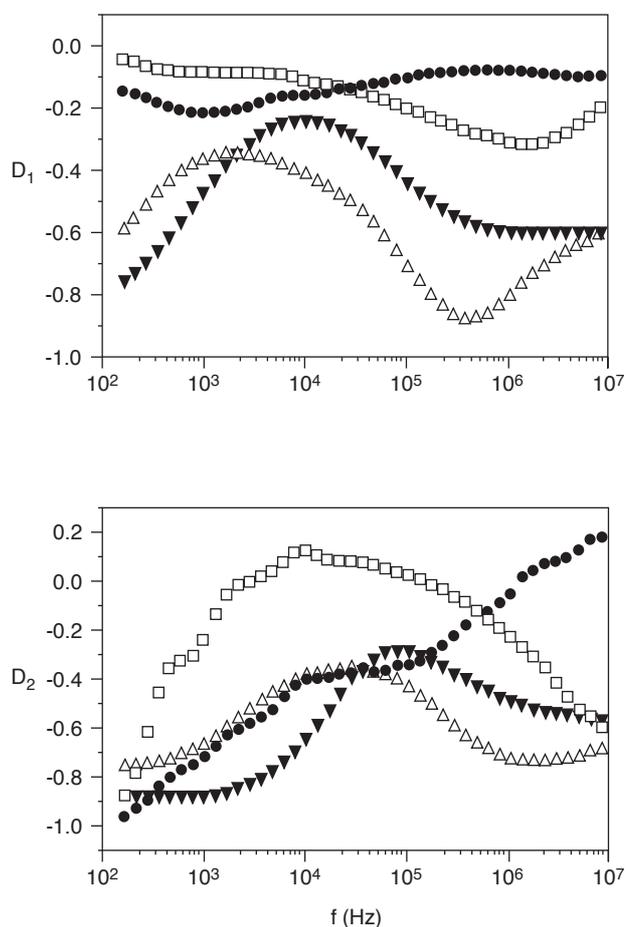

Figure 8

Plot of D_1 and D_2 as a function of frequency for glass. Open square: oil wet sample saturated with deionized water (g4A). Solid dot: oil wet sample saturated with brine (g4C). Open up triangle: water wet sample saturated with deionized water (g4E). Solid down triangle: water wet sample saturated with brine (g4H).
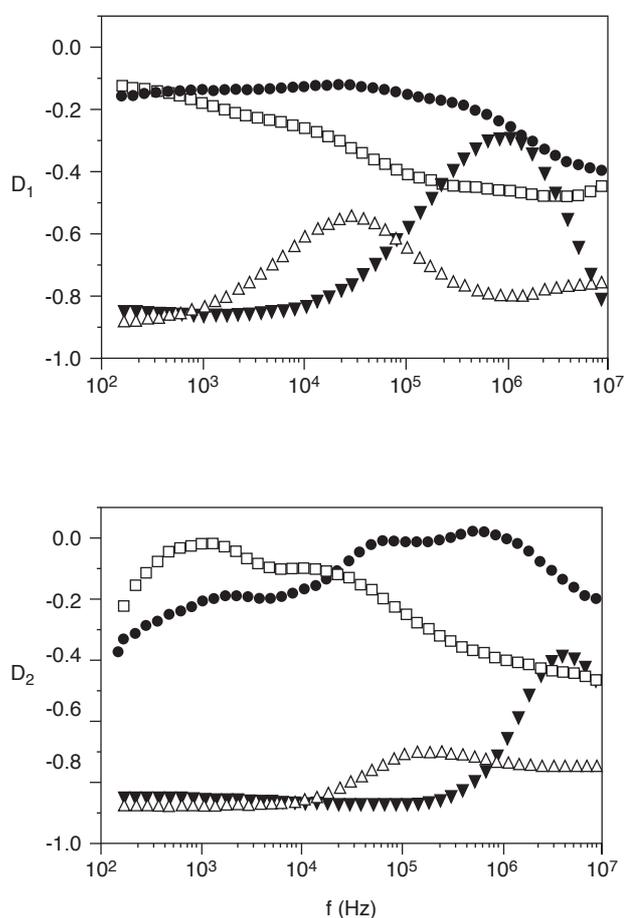
Figure 9

Plot of D_1 and D_2 as a function of frequency for Berea. Open square: oil wet sample saturated with deionized water (beB). Solid dot: oil wet sample saturated with brine (beC). Open up triangle: water wet sample saturated with deionized water (beF). Solid down triangle: water wet sample saturated with brine (beH).

3.4 The Loss Tangent

The loss tangent is another parameter which makes it possible to distinguish between a water wet condition and an oil wet condition. The loss tangent is defined as $\tan(\delta) = \varepsilon''/\varepsilon'$, and it is related to the ratio of the energy dissipated per radian in the material to the energy stored at the peak of polarization by the electric field. The behaviors of $\tan(\delta)$ as a function of frequency for some samples of glass and Berea are shown in Figures 10 and 11.

As observed for the dispersivity, the electrical response of the water wet samples is dominated, at low frequencies, by a Power Law. The dielectric permittivity is asymptotic to $-i\sigma_{dc}/(\varepsilon_0\,\omega) + A(i\omega)^{N-1}/\varepsilon_0$ for $\omega \rightarrow 0$ ($0 < N < 1$). As the frequency increases $\tan(\delta)$ decreases and then rises, showing a peak in the range of frequencies where MW relaxation dominates. Only the left end of the peak is visible for some samples, since the peak frequency is greater than 10 MHz. We believe that this peak is due to Maxwell-Wagner relaxation.

When comparing the samples saturated with brine with the samples saturated using deionized water, it is found that in the former the $\tan(\delta)$ peak occurs at higher frequencies. As previously noted, this is in qualitative accordance with Equation (3a), which shows that the relaxation time is inversely proportional to the conductivity of the saturating water. This results in a shift of the $\tan(\delta)$ peak towards high frequencies for the samples saturated with brine. $\tan(\delta)$ assumes distinctly lower values in oil wet samples than in water wet samples, in the range of frequencies where the MW peak occurs. This difference is clearly visible when the peak intensity associated with MW relaxation is observed; the $\tan(\delta)$ peak has a value lower by at least a factor of 10 in the oil wet samples than the corresponding value observed for water wet samples. The peak is also considerably broader in water wet samples. For example, in oil wet Berea samples saturated with deionized water the $\tan(\delta)$ value falls by half the peak intensity in a frequency range of 5 orders of magnitude, whereas 2 orders of magnitude are sufficient for the corresponding water wet samples. The weak intensity of the peak, combined with its broad extension implies lower dispersivity in oil wet systems than in water wet systems.
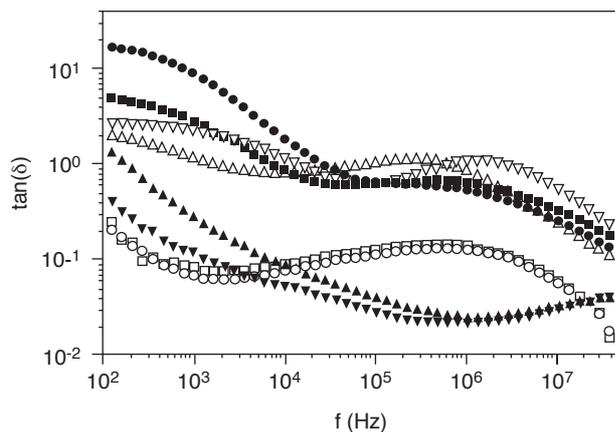
Figure 10

Log-log plot of the loss tangent $\tan(\delta)$ as a function of frequency for glass. Open square and circle: oil wet samples saturated with deionized water (g4A and g4B). Solid up and down triangle: oil wet samples saturated with brine (g4C and g4D). Open up and down triangle: water wet samples saturated with deionized water (g4E and g4F). Solid dot and Solid square: water wet samples saturated with brine (g4G and g4H).
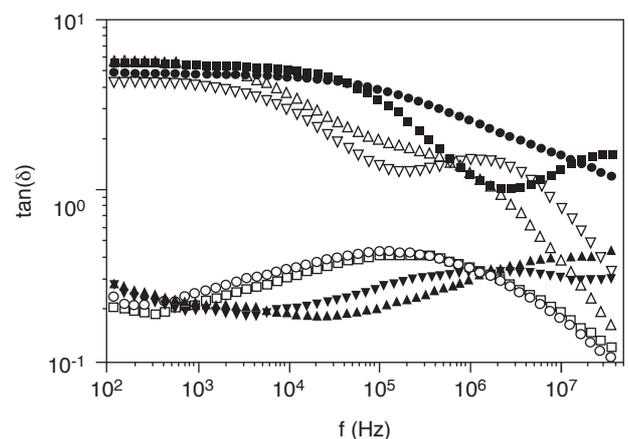
Figure 11

Log-Log plot of the loss tangent $\tan(\delta)$ as a function of frequency for Berea. Open square and circle: oil wet samples saturated with deionized water (beA and beB). Solid up and down triangle: oil wet samples saturated with brine (beC and beD). Open up and down triangle: water wet samples saturated with deionized water (beE and beF). Solid dot and solid square: water wet samples saturated with brine (beG and beH).

CONCLUSIONS

The electric response of glass filters and Berea sandstone was analyzed in the interval 10^2-10^8 Hz and the effect of wettability on the measured properties was investigated. Both strongly water-wet and strongly oil-wet samples were tested and showed markedly different responses. The dispersivity and the loss tangent were found to be the most suitable parameters for an indirect determination of wettability.

We can draw the following conclusions from this study:

– At low water saturation, the dielectric properties of the rock are influenced firstly by the distribution of water and oil in the pore space.

– Other parameters such as porosity, the level of saturation and water conductivity, appreciably affect the actual value of all electrical properties, but have a secondary effect on the frequency behavior of the electrical response of the system.

– At low water saturation, water wet systems have distinctly noticeable electrical responses compared with oil wet systems, irrespective of the value assumed by the above parameters.

– The dispersivity coefficients D_1 and D_2 and the loss tangent $\tan(\delta)$ are the electrical parameters that are best able to distinguish between a water wet condition and an oil wet condition.

– A water wet situation is essentially recognizable by three factors: a significant contribution of the dispersive transport governed by a power law; distinctly higher $\tan(\delta)$ values throughout the frequency range; and a much higher dispersivity, measured by the D_1 and D_2 coefficients.

NOMENCLATURE

$\varepsilon(\omega) = \varepsilon'(\omega) - i\varepsilon''(\omega)$ generalized complex permittivity

$\varepsilon_P(\omega) = \varepsilon_P'(\omega) - i\varepsilon_P''(\omega)$ complex permittivity associated with polarization effects

$\varepsilon_{PL}(\omega) = \varepsilon_{PL}'(\omega) - i\varepsilon_{PL}''(\omega)$ complex permittivity related to charge transport (PL)

$\varepsilon_L(\omega) = \varepsilon_L'(\omega) - i\varepsilon_L''(\omega)$ complex permittivity defined by the Lysne's model

ε_0 permittivity of empty space

ε_∞ unrelaxed dielectric constant

ε_m dielectric constant of the oil

ε_w dielectric constant of the water

ε_S static dielectric constant of the sample

$\Delta\varepsilon = \varepsilon_\infty - \varepsilon_S$ relaxation strength

σ_{dc} dc conductivity of the sample

σ_w dc conductivity of the water

τ relaxation time

ϕ rock porosity

S_w water saturation

β shape parameter of the water inclusions

g inclusion orientation factor

C_0 capacitance of the empty cell

C_X capacitance of the wires

$Y_C(\omega) = [Z_C(\omega)]^{-1}$ admittance of the cell and interconnecting wires

$Y_0(\omega) = [Z_0(\omega)]^{-1}$ admittance of the empty cell

Z_I electrode-sample interface impedance

Z_S sample impedance

Z_L series impedance of the wires

$Z_r = [i\omega\varepsilon(\omega)C_0]^{-1} = Z_S + Z_I$ impedance of the system cell + sample

A effective cross-section of the sample

l sample thickness

$\rho_a = \rho_a' + i\rho_a'' = Z_r \cdot A/l$ complex resistivity of the sample

$D_1 = d[\text{Log}(\varepsilon' - \varepsilon_\infty)]/d(\text{Log}\,\omega)$ dispersivity parameter

$D_2 = d(\text{Log}\,\varepsilon'')/d(\text{Log}\,\omega)$ dispersivity parameter

$\tan(\delta) = \varepsilon''/\varepsilon'$ loss tangent.

REFERENCES

1   Sen P.N., Scala C. and Cohen M.H. (1981) A self-similar model for sedimentary rocks with application to the dielectric constant of fused glass beads. *Geophysics*, 46, 5, 781-795.

2   Kenyon W.E. (1984) *Journal of Applied Physics*, 55, 3153-3159.

3   Knight R. and Nur A. (1987) The dielectric constant of sandstones, 60 kHz to 4 MHz. *Geophysics*, 52, 5, 644-654.

4   Haslund E., Hansen B.D., Hilfer R. and Nøst B. (1994) *Journal of Applied Physics*, 76, 5473-5480.

5   Nettelblad B. and Niklasson G.A. (1996) The dielectric dispersion of liquid-filled porous sintered materials. *J. Phys.: Condens. Matter*, 8, 2781-2790.

6   Sillars R.W. (1937) *J. Inst. Elec. Eng.*, 80, 378-394.

7   Taherian M.R., Kenyon W.E. and SafinyaK. A. (1990) Measurement of dielectric response of water-saturated rocks. *Geophysics*, 55, 12, 1530-1541.

8   Lysne P.C. (1983) A model for the high-frequency electrical response of wet rocks. *Geophysics*, 48, 6, 775-786.

9   Lockner D.A. and Byerle J.D. (1985) Complex resistivity measurements of confined rock. *Journal of Geophysical Research*, 90, 7837-7847.

10   Börner F.D. (1992) Complex conductivity measurements of reservoir properties. *Advances in core evaluation III - Reviewed Proceedings of the 3rd SCA Symposium*, Gordon and Breach Science Publishers, 359-386.

11   Börner F.D. (1997) Combined complex conductivity and dielectric measurements on core samples. *SCA Paper No. 9736 presented at the 1997 SCA International Symposium*, Calgary.

12   Glover P.W.J., Meredith P.G., Sammonds P.R. and Murrel S.A.F (1994) Ionic surface electrical conductivity in sandstone. *Journal of Geophysical Research*, 99, 21635-21650.

13   Jonscher A.K. (1983) *Dielectric Relaxation in Solids*, Chelsea Dielectric Press, London.

14   Jonscher A.K. (1996) *Universal Relaxation Law*, Chelsea Dielectric Press, London.

15   Dissado L.A. and R.M. Hill (1984) *J. Chem. Soc. Faraday Trans.*, 2, 80, 291-319.

16   Wong P. (1987) Fractal Surfaces in Porous Media. *Physics and Chemistry of Porous Media*, AIP, New York, 304-318.

17   Ruffet C., Gueguen Y. and Darot M. (1991) Complex conductivity measurements and fractal nature of porosity. *Geophysics*, 56, 6, 758-768.

18   Takach N.E., Bennett L.B. and Douglas C.B. (1989) Generation of oil-wet model sandstone surfaces, *SPE Paper No. 18465 presented at the 1989 International Symposium on Oilfield Chemistry*, Houston.

19   MacDonald J.R. (1987) *Impedance Spectroscopy*, J. Wiley and Sons, New York.

20   Da Rocha B.R. and Habashy T.M. (1997) Fractal geometry, porosity and complex resistivity: from rough pore interfaces to hand specimens. *Developments in Petrophysics*, edited by M.A. Lovell and P.K. Harvey, Geological Society Special Publication No. 122, London, part I, 277-286, part II, 287-97.

21   Hilfer R. (1991) Geometric and dielectric characterization of porous media. *Physical Review*, B, 44, 60-75.

Final manuscript received in October 1998